**Abstract** Optical frequency combs enable precision measurements in fundamental physics and have been applied to a growing number of applications, such as molecular spectroscopy, LIDAR and atmospheric trace-gas sensing. In recent years, the generation of frequency combs has been demonstrated in integrated microresonators. Extending their spectral range to the visible is generally hindered by strong normal material dispersion and scattering losses. In this paper, we report the first realization of a green-light frequency comb in integrated high-Q silicon nitride (SiN) ring microresonators. Third-order optical non-linearities are utilized to convert a near-infrared Kerr frequency comb to a broadband green light comb. The 1-THz frequency spacing infrared comb covers up to 2/3 of an octave, from 144 to 226 THz (or 1327-2082 nm), and the simultaneously generated green-light comb is centered around 570-580 THz (or 517-526 nm), with comb lines emitted down to 517 THz (or 580 nm) and up to 597 THz (or 502 nm). The green comb power is estimated to be as high as -9.1 dBm in the bus waveguide, with an on-chip conversion efficiency of -34 dB. The proposed approach substantiates the feasibility of on-chip optical frequency comb generation expanding to the green spectral region or even shorter wavelengths.
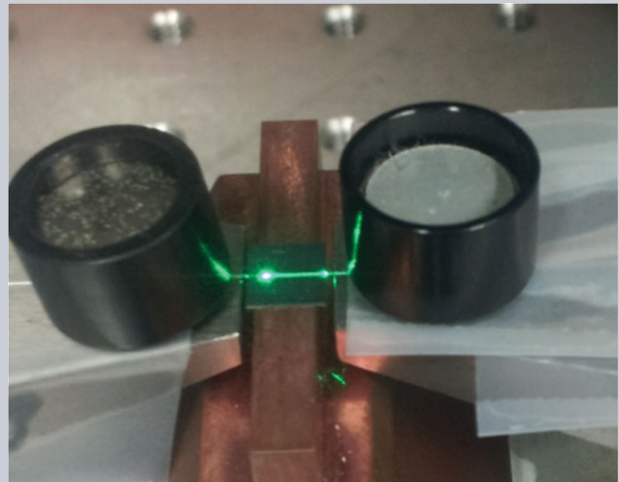
ORIGINAL PAPER

Frequency comb generation in the green using silicon nitride microresonators

Leiran Wang[1,2,†], **Lin Chang**[1,†], **Nicolas Volet**[1,*,†], **Martin H. P. Pfeiffer**[3], **Michael Zervas**[3], **Hairun Guo**[3], **Tobias J. Kippenberg**[3], and **John E. Bowers**[1]

1. Introduction

Thanks to the availability of complementary metal-oxide semiconductor (CMOS) fabrication technology and the property of high index contrast, silicon photonics has become one of the most promising photonic integration platforms [1–3]. Ring microresonators play a crucial role in the success of silicon photonics, benefiting from the unprecedented small chip size and high build-up energy inside the resonator with strong confinement [4–6]. Enormous development has been achieved concerning microresonator-based functional devices [7–11]. One technologically promising application of ring microresonators is the generation of an optical frequency comb (OFC) using parametric frequency conversion. OFCs are a cornerstone in precision measurement in fundamental physics, such as the optical clocks and absolute frequency metrology [12,13], but are equally important in many practical applications. The majority of this research was primarily focused on the infrared (IR) region and progress has been achieved, including the octave-spanning OFC that could be used in f-$2f$ self-reference systems [14], ultra-high repetition-rate soliton generation [15–17], and coherent terabit communications [18]. Besides IR wavelengths, OFCs working at visible wavelengths can enable other applications, such as enabling comb locking to optical atomic transitions that are critical for realization of optical atomic clocks, as well as biological imaging [19] or optical coherence tomography.

Ultra-broadband visible-to-IR supercontinuum generation in SiN integrated optical waveguides has been demonstrated [20,21]. However, visible comb generation is limited by the strong normal material dispersion, as well as the increase in Rayleigh scattering at short wavelengths that may reduce the quality factor Q of microresonators. Generally, anomalous group-velocity dispersion (GVD) is required to

[1] Department of Electrical and Computer Engineering, University of California, Santa Barbara (UCSB), CA, 93106, USA
[2] State Key Laboratory of Transient Optics and Photonics, Xi'an Institute of Optics and Precision Mechanics, Chinese Academy of Sciences, Xi'an 710119, China
[3] École Polytechnique Fédérale de Lausanne (EPFL), 1015 Lausanne, Switzerland
[†] Co-first authors
[*] Corresponding author(s): e-mail: volet@ece.ucsb.edu

phase-match parametric oscillations mediated by the Kerr nonlinearity induced four-wave mixing (FWM) [7, 15, 16]. However, in the visible, the normal material dispersion becomes too strong to be compensated by waveguide dispersion, which results in overall normal GVD. Additionally, the lower Q that is expected to occur due to Rayleigh scattering at the waveguide sidewalls may reduce the cavity enhancement of the power. This in turn may hinder efficient OFC generation [19] due to the inverse quadratic dependence of parametric oscillation threshold on Q. Previous demonstrations of octave-spanning combs pumped in the IR have been reported beyond 2 μm (corresponding to a frequency of 149.9 THz) on the long-wavelength side, but failed to extend the short-wavelength side into the visible [14]. Recent work extended such microresonator combs to the visible. In particular, 7 red and green comb lines were observed with a high-Q aluminum nitride (AlN) ring microresonator and attributed to second-harmonic (SH), sum-frequency (SF) and third-harmonic (TH) generations [22]. With the Si-based platform that leverages the cost-effective and excellent compatibility of the widespread CMOS fabrication technology, close-to-visible comb operation was achieved with a Si_3N_4 ring microresonator, where 17 comb lines were observed near 770 nm (or 389 THz) and attributed to SHG and SFG [19]. In the green spectral range, THG-induced frequency conversion into a single spectral line near 520 nm (or 577 THz) was previously reported [23], but no comb in the visible green region has been reported so far.

In this work, we demonstrate the first green light comb (GLC) generation in SiN ring microresonators. THG and third-order SFG effects are utilized to convert the IR frequency comb into the visible GLC. By optimizing the waveguide geometry, phase matching is achieved between an IR pump mode and visible higher-order modes. Compared to the generation of visible combs from phase-matching of a single higher-order mode [22], the present approach enables a much broader and a more efficient frequency conversion into the green spectral region. The generated GLC, converted from an IR frequency comb pumped at 192 THz (or 1561 nm), is centered around 570-580 THz (or 517-526 nm). The measured output power of the GLC is as high as −19.6 dBm (or 11 μW) and its power is estimated to −9.1 dBm (or 123 μW) in the bus waveguide. This yields an on-chip conversion efficiency of about −34 dB (or $4 \cdot 10^{-4}$). This approach extends the range of accessible frequencies using parametrically generated Kerr combs to the visible range, that may find applications in chip-scale optical clock and the creation of a coherent link between IR and visible spectral ranges. Moreover, the generated GLC may directly be used in $2f$-$3f$ self-referencing schemes [24].

2. Device description

The devices are fabricated by low-pressure chemical vapor deposition (LPCVD) on a Si substrate. The photonic Damascene process [25] is used to deposit an 850-nm thick near stoichiometric Si_3N_4 layer on a prestructured substrate that includes a dense stress release pattern next to the actual waveguide pattern. Crack formation that causes high scattering losses in the waveguide is effectively prevented as the dense substrate topography suppresses stress buildup in the thin film. The Si_3N_4 waveguide is cladded to the bottom and to the top by a 3-μm thick SiO_2 layer. A top view schematic and an SEM picture of the investigated device are shown in Fig. 1(a) and Fig. 1(b), respectively. The microresonator waveguide width H is set to 1.6 μm, while the ring radius R is 22.85 μm, corresponding to a free spectral range (FSR) of ∼1 THz. The bus waveguide width W is 0.1 μm. Different coupling strength can be achieved by varying the gap G between the bus and the ring waveguides. Critical coupling is experimentally achieved for $G = 750$ nm. A typical TE transmission spectrum is shown in Fig. 1(c) and Fig. 1(d). The measured 3-dB frequency bandwidth of the resonance near the critical coupling condition is $\Delta f_{1/2} \cong 140$ MHz. The loaded Q factor, extracted from the full width at half depth, is $Q \cong 1.30 \cdot 10^6$. A resonance measured for a TM input polarization is shown in Fig. 1(e), with $Q \cong 2.59 \cdot 10^5$.

3. Simulations

In order to realize broadband (octave-spanning) frequency comb generation, dispersion engineering of the waveguide's group velocity dispersion (GVD) is necessary [7, 8, 13–16, 26]. By tailoring the width and the height of the waveguide, the normal material dispersion of Si_3N_4 at 1.55-μm telecom wavelength can be compensated by an anomalous waveguide dispersion.

The angular frequencies of the resonances for the ring microresonator can be approximated with the following Taylor series [15, 27]:

$$\omega_\mu = \omega_0 + D_1\mu + \frac{1}{2}D_2\mu^2 + \sum_{m>2}\frac{1}{m!}D_m\mu^m, \quad (1)$$

where ω_0 is the angular frequency of the pumped center mode and μ is the relative mode order. In particular, when $D_m = 0$ for all $m > 2$, $D_1/(2\pi)$ is related to the FSR of the microresonator at ω_0 and $D_2/(2\pi)$ is the difference between two adjacent FSRs from one pair of resonances to the next one. The GVD β_2 is related to the parameters D_1 and D_2 via [15, 28]:

$$D_2 = -\frac{c}{n_g}D_1^2\beta_2, \quad (2)$$

where n_g is the group effective index of the resonator at ω_0 and c is speed of light in vacuum. Fig. 2 shows the simulated dispersion profile featuring anomalous dispersion ($D_2 > 0$) around the pump frequency of 193 THz (corresponding to 1.55 μm wavelength).

The dispersion is optimized to yield broadband combs. The waveguide dispersion of the Si_3N_4 ring microresonators is also designed to simultaneously phase-match the IR comb and its frequency-tripled GLC. Efficient THG can
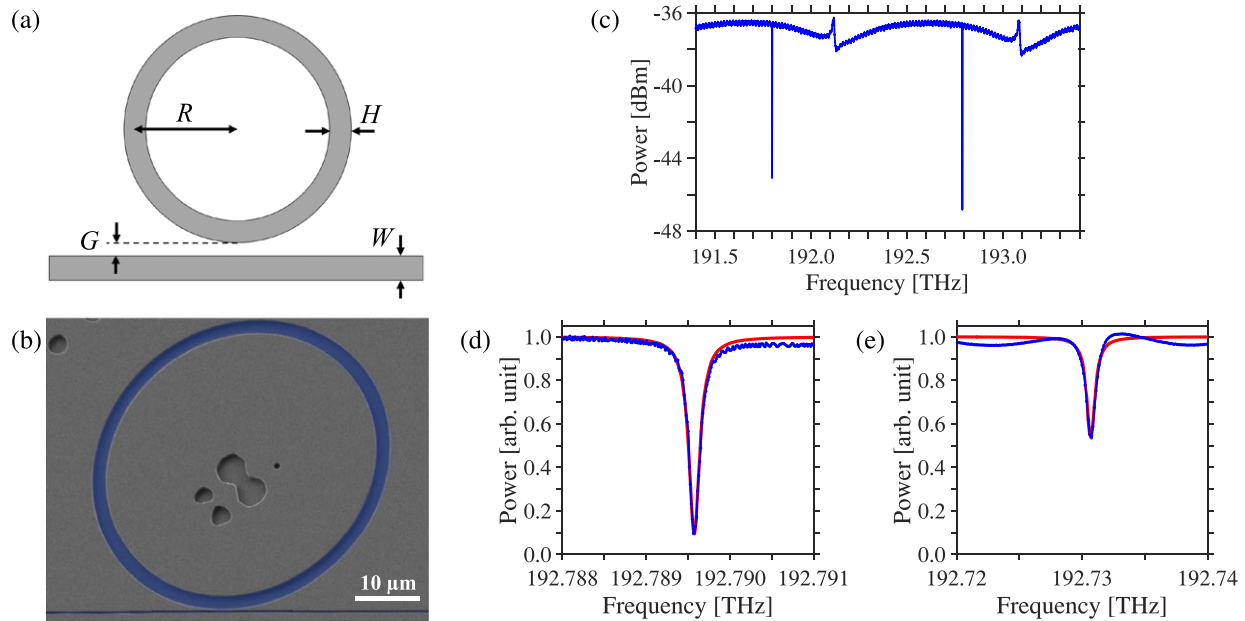
Figure 1 (a) Top-view schematic and (b) SEM picture of the ring microresonator with the bus waveguide. The features visible in the central and the top left parts of (b) are remains of the stress relax checkerboard pattern. (c) Transmission spectrum measured at low EDFA power (-13 dBm) for a TE input polarization, and (d) fitting (in red) of the resonance near 192.8 THz (corresponding to a wavelength of $\sim$1555 nm). (e) Fitting (in red) of a resonance measured for a TM input polarization.
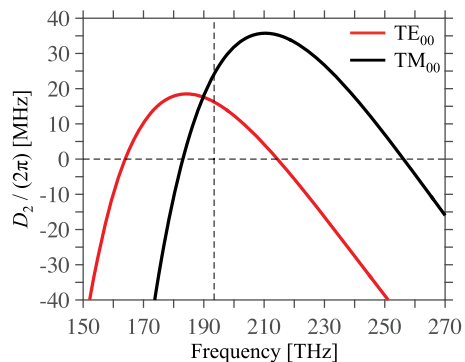
Figure 2 Simulated spectra of the second-order dispersion $D_2/(2\pi)$ for the fundamental TE (in red) and TM (in black) modes. The vertical dashed line indicates the 1.55-μm wavelength.

be achieved if the wavenumber $k = 2\pi n f/c$ of the fundamental waveguide mode at the IR frequency f_p is 3 times smaller than the wavenumber of a higher-order mode at the green frequency $3f_p$ [23]. The effective indices n and the intensity distributions for the fundamental TE and TM modes at the pump frequency, and for higher-order modes at the TH frequency are simulated with FIMMWAVE [29]. The design parameters used in the simulations are the same as those for the fabricated ring microresonators, and the results for the phase-matching conditions are shown in Fig. 3. It can be seen that at some frequencies, the effective index of several higher-order TH modes matches the effective index of the fundamental TE or TM mode. Specifically, there are three matching conditions between the 18th, 19th, 20th TH
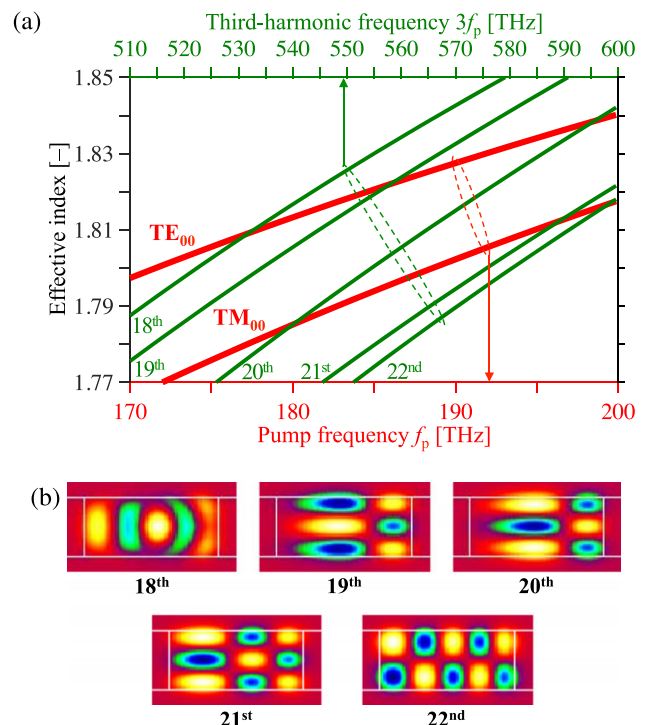
Figure 3 (a) Simulated spectra of the effective index for the fundamental TE and TM modes of the ring microresonator (in red) at the pump frequency f_p, and for higher-order modes (18th to 22th orders, in green) at the third-harmonic frequency. (b) Cross-section of the intensity distributions in the ring resonator simulated for the relevant higher-order modes at 576.5 THz (or 520 nm).

modes and the fundamental TE mode (for $f_p \cong 177.4$ THz, 186.2 THz and 198.5 THz), as well as three other matching conditions between the 20th, 21th and 22th TH modes and the fundamental TM mode (for $f_p \cong 180.1$ THz, 196.6 THz and 199.2 THz). Each matching condition contributes to broadening the spectral range in the frequency-converted GLC lines.

4. Experimental results and discussions

A tunable single-frequency CW laser (Agilent 81642A, with a typical linewidth of ∼100 kHz and a tuning range of 1510-1640 nm) is used as the seed laser to pump the ring microresonator. An erbium-doped fiber amplifier (EDFA, IPG EAR-2K-C) with a maximum output power of ∼33 dBm ($\cong$ 2 W) is used to boost the pump power. A polarization controller is positioned before the input lensed fiber to selectively couple into the fundamental TE or TM mode of the waveguide. The light is coupled in and out of the device through tapered lensed fibers (OZ optics, with a spot diameter of 2 μm, a working distance of 12 μm and an anti-reflective coating designed for 1.55 μm wavelength). The signal intensities in the IR and in the green spectral region are monitored respectively by a high-speed 1550-nm power sensor and by a silicon-PIN photo-detector for visible light. Two optical spectrum analyzers (Yokogawa AQ6375 for 1200-2400 nm and AQ6373B for 350-1200 nm) are used to measure their respective spectra. Using the thermal-locking technique [30], IR Kerr comb can be obtained when the pump frequency is tuned into the resonance, with an input power larger than the threshold for parametric oscillations. As the laser scans into the resonance, the buildup of power inside the ring microresonator can lead (via degenerate or non-degenerate FWM) to the generation of broadband Kerr frequency combs [7]. For this excitation pathway, it is noted that the comb is in the high-noise regime [15]. While not attempted or observed in this work, low-noise comb states can be attained by techniques, such as δ-Δ matching or parametric seeding, or via the soliton regime [16].

4.1. Green-light comb formation

The threshold value of on-chip input power for THG generation (only one frequency line in green) is estimated to as low as ∼16 dBm, and the threshold for GLC generation (with several green lines) is ∼20 dBm. The observed formation process for the IR comb and the simultaneously converted GLC is detailed in Fig. 4. The data from Fig. 4(a) suggest that the first (central) emitted line of the GLC is formed by the THG process, where the interaction of three photons with frequency f_p from the IR pump laser results in the creation of a photon with the tripled frequency $3f_p$. Tuning the pump frequency gradually into resonance, both the number and the intensity of the IR comb lines increase
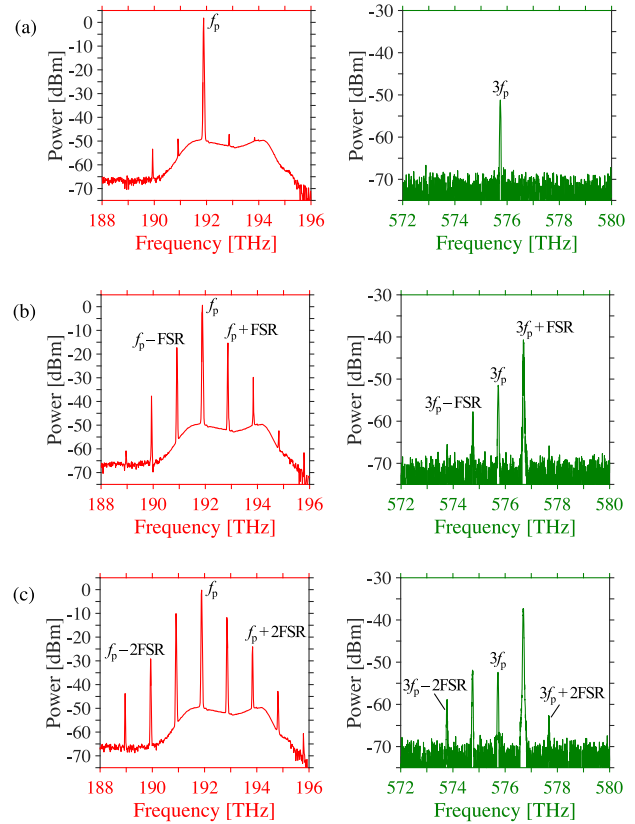
Figure 4 Generation process of the IR Kerr comb (left column) and the simultaneously emitted GLC (right column), by gradually tuning the TE-polarized IR pump to the resonance near $f_p \cong 191.9$ THz. The IR comb and the GLC both have FSRs near 975 GHz. The first line of the GLC (at $3\,f_p$) is thought to be created by THG, and the additional lines (at $3\,f_p + \nu$FSR) by third-order SFG.

as the cavity circulating power strengthens. Ideally, their frequencies can be expressed by [15]:

$$f_{\mu,\mathrm{IR}} = f_p + \mu\,\mathrm{FSR}, \tag{3}$$

where f_p is the pump frequency, μ is the relative mode order of the IR comb lines with a frequency spacing equal to the free spectral range FSR. It is noted that this equation only describes the ideal, coherent operation regime and specifically disregards the formation of sub-combs. In the latter case, the comb lines broaden and thus only approximately satisfy relation (3) in the present, high-noise case. The high noise of the incoherent comb state has two effects on the GLC. First, the noise is transferred to the GLC, which broadens its lines and induces excess noise. A second effect is the reduced peak power compared to *e.g.* a soliton state. The latter has pulses traveling within the cavity and thus locally higher peak power and more efficient non-linear processes.

It can be seen from Fig. 4(b) and Fig. 4(c) that as the IR comb lines strengthen, more green comb lines are simultaneously generated. Assuming that the additional lines

of the GLC were also created by THG, the FSR of the GLC would be 3 times larger than that of the IR comb. However, the GLC and the IR comb have the same FSR (∼1 THz). This indicates that the additional lines of the GLC are created by the third-order SFG process, where the interaction of three photons from the IR comb, with respective frequencies $f_{\mu_1,\mathrm{IR}}$, $f_{\mu_2,\mathrm{IR}}$ and $f_{\mu_3,\mathrm{IR}}$ (with the convention: $|\mu_1| \leq |\mu_2| \leq |\mu_3|$), results in the creation of a photon in the green, with a frequency ideally given by:

$$f_{\nu,\mathrm{green}} = 3f_p + \nu\,\mathrm{FSR}, \qquad (4)$$

where $\nu = \mu_1 + \mu_2 + \mu_3$ is the relative mode order of the GLC line. Indeed, it is suggested [19, 22] that if the phases of the generated IR sidebands relative to the pump are fixed, the phase relationship of the converted GLC will be correspondingly fixed and determined by the IR comb frequency spacing. In this ideal case, the newly generated components will thus be equidistant in frequency domain with respect to the IR pump. In addition, the parametric processes can be efficiently enhanced only when these frequencies coincide with the modes of the ring microresonator [3, 7]. The phase-matching condition would thus be automatically satisfied once it is ensured for both the FWM of the IR comb and the THG of the central line of the GLC, and it would successively lead to a cascaded frequency-tripling process through the third-order SFG.

It is worth reminding that the generation of the IR Kerr comb is based on the FWM process, where the interaction of two pump photons (or two IR comb photons with different frequencies) results in the creation of a new pair of photons with blue- and red-shifted frequencies [7,19]. This type of FWM-based process is highly unlikely to explain the generation of the extra lines of the GLC. Indeed, the intensity of its central line (at the frequency $3f_p$) is not expected to reach the threshold power P_{th} for parametric oscillations [22,23]. Even though P_{th} is inherently small in high-Q microresonators, losses due to Rayleigh scattering (inversely proportional to the fourth power of the wavelength) would still result in a high value for the threshold power of the GLC based on FWM. The strong normal material dispersion would also hinder the generation of a Kerr comb in the green spectral region. Furthermore, as seen in Fig. 4(b) and Fig. 4(c), the central line of the GLC is generally not the most intense. This feature could not be accounted for, if the generation of the extra lines of the GLC were based on FWM of the line at $3f_p$. In particular, the data of Fig. 4(b) suggest that two photons from the IR pump laser ($\mu_1 = \mu_2 = 0$) interact with one photon from the IR Kerr comb at the mode $\mu_3 = \pm 1$ to contribute to the line of the GLC with $\nu = \pm 1$. This enhanced third-order non-linear parametric process takes advantage of direct interaction with the strong pump instead of merely depending on the newly generated THG line. High GLC power is then observed, with reduced constrains on the pump power.
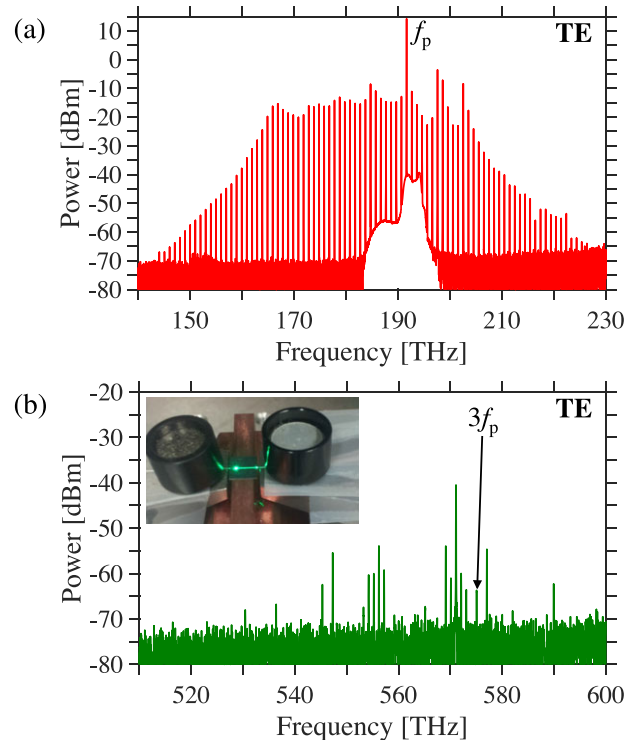
Figure 5 (a) IR Kerr comb generated with a TE pump and (b) the corresponding GLC with 18 spectral lines. In (b), the inset shows a photograph of the probed device. The pump frequency $f_p = 191.7$ THz and both IR and green combs have FSR $\cong 992.6$ GHz.

4.2. Influence of the input polarization

At the maximum output power of the EDFA (∼33 dBm $\cong$ 2 W), broadband albeit high-noise IR combs can be established. By carefully positioning the input fiber and optimizing the polarization, the combs are observed with different features with the fundamental (quasi-)TE or (quasi-)TM mode pumping. For the TE situation, as shown in Fig. 5, the observed IR comb exhibits a uniform envelope and covers 2/3 of an octave (144-226 THz or 1327-2082 nm). The corresponding GLC consists of 18 lines that spread from 530 THz to 590 THz (or 508-566 nm). The measured frequency spacing for the IR comb and the GLC are both FSR $\cong$ 992.6 GHz. Ideally the GLC would be continuous and uniform; however, some comb lines are missing in the spectrum shown in Fig. 5(b), which can be attributed to a resonance mismatch [19]. Besides, the simulations of Fig. 3 showed that phase-matching of a TH mode can be realized with different IR comb lines. As a result, several separated spectral clusters are observed in Fig. 5(b) with distinct strong peaks. The first and second strongest GLC lines are located at 571.1 THz and 577.0 THz, respectively. However, the pump frequency if $f_p = 191.7$ THz, corresponding to the THG frequency of $3f_p = 575.1$ THz. For THG, all 3 input photons are provided from the same IR comb line. When computing the efficiency bandwidth, the frequency of these 3 photons thus varies simultaneously. In
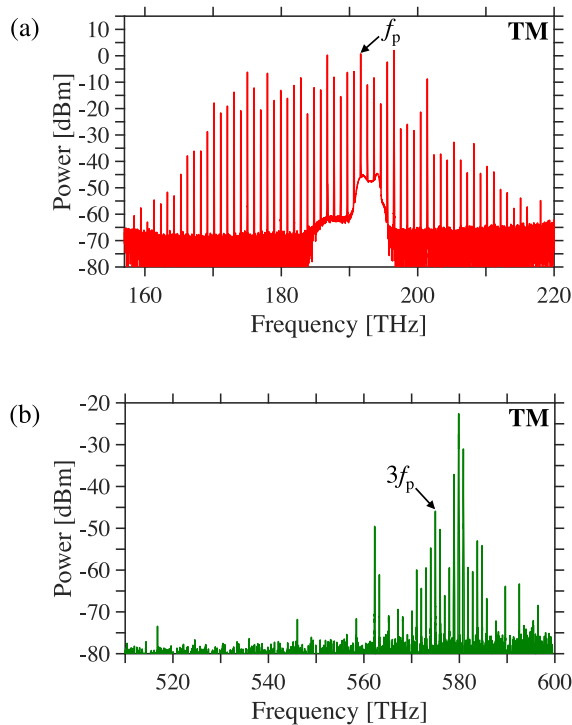
Figure 6 (a) IR Kerr comb generated with a TM pump and (b) the corresponding GLC with 30 spectral lines. In (b), the inset shows a photograph of the probed device. The pump frequency $f_p = 191.6$ THz and both IR and green combs have FSR $\cong$ 977.2 GHz.

contrast, for third-order SFG, the frequency of one or two input photons is fixed at the pump of the IR comb, and the frequencies of photons from other comb lines vary. Therefore, the phase-matching condition for third-order SFG is less dependent on dispersion, which is similar to the effects reported in Ref. [19]. This implies that the phase-matching requirement for the third-order SFG is less stringent than that for THG, which enables the conversion of a broader bandwidth of IR comb lines into the wider visible range. This effect is responsible for the broad bandwidth of the GLC and the nearly continuous comb lines observed experimentally

From the simulations of Fig. 3, the phase-matched window with the fundamental TM mode has a better overlap with the effective working bandwidth of the employed EDFA (191-196 THz, or 1530-1570 nm) compared with that of the TE mode. This can explain why much stronger GLC is achieved in the experiments with the fundamental TM mode pumping, as shown in Fig. 6. The generated IR comb extends over a narrower range (158-218 THz, or 1375-1897 nm) compared to the case of TE pumping. Yet, 30 lines are detected for the GLC, with frequencies ranging from 517 THz to 597 THz (or 502-580 nm). In the central part of the THG frequency, 17 continuous comb lines are observed, as seen in Fig. 6(b). Both IR comb and GLC have FSR $\cong$ 977.2 GHz.

With TE pumping, the output power of the GLC measured with the photo-detector is about −35.2 dBm (or 0.3 µW). Losses due to coupling and propagation of the green light are estimated to 10.7 dB. Therefore, the power of the GLC in the output bus waveguide is about −24.5 dBm (or 3.5 µW). With TM pumping, the GLC power measured with the photo-detector is about −19.6 dBm (or 11 µW), and its power in the output bus waveguide is estimated to −9.1 dBm (or 123 µW). The pump power in the input bus waveguide is estimated to 25 dBm (or 316 mW), thus yielding an on-chip conversion efficiency of −34 dB (or $4 \cdot 10^{-4}$). The net efficiency is −53 dB (or $6 \cdot 10^{-6}$), thus more than 3 orders of magnitude larger than recently reported with AlN ring microresonators [22].

At high EDFA power (33 dBm), the transmitted power for TE is larger than for TM [see Fig. 5(a) and Fig. 6(a)]. This suggests that the extinction ratio for TM is higher than for TE , which is opposite to what we observe at low power. This difference can be explained as follows. The extinction ratio may change in the case of non-linear interactions inside the resonator, which transfer power from the central pump mode to the adjacent lines of the comb. This nonlinear mixing acts like an additional loss term to the central mode, which changes the extinction ratio of the central comb line. The TM mode is believed here to be over-coupled, which in general results in a much higher efficiency at high powers. Indeed, in the over-coupled case, this additional non-linear loss drives the resonance towards the full extinction of a critically coupled resonance and thus to the highest possible efficiency. Therefore, more power is built-up in the ring resonator for TM. We think that this is one of the reasons that explain why the GLC generation has a higher efficiency for TM. In addition, the TM mode shows in general (experimentally and in simulations) much higher coupling strength to the micro-resonator. This is due to a more favorable field overlap integral.

We chose the actual pump frequency that maximizes the green light intensity. One reason why this frequency does not perfectly match the value predicted from the phase-matching condition of Fig. 3 is due to the mismatch of the resonances. As the resonator has a large FSR (1 THz) and a high quality factor in the IR ($Q \cong 1.4 \cdot 10^6$), the 3-dB bandwidth of the IR resonance is narrow (140 MHz). Therefore, the best phase-matching condition may not be the resonant frequency for IR and the green light correspondingly.

The best phase matching condition is also very sensitive to fabrication, which has tolerance of up to 50 nm on vertical and horizontal dimensions for these samples. As shown in Fig. 3, a refractive index change of 0.01 can shift the best phase-matching frequency by several THz. The actual pump may thus be a little bit off from the simulation value.

The thermally induced shift may also be a reason for this difference. We indirectly observe a difference between thermally induced resonance drifts at IR and green frequencies. In particular, certain green comb lines that occur at low pump power (which requires good phase-matching and resonance conditions at these frequencies) decrease in intensity or even disappear when the pump power is increased. This suggests that the phase-matching and resonance

conditions of the two frequencies drift, which influences the GLC efficiency.

There is a balance between the Q value and the resonance condition, for highly efficient THG processes. As long as the phase-matching and resonance conditions at both pump and green frequencies are perfectly satisfied, higher Q are expected to yield better efficiency. However, as the overlap mismatch is an issue, a lower Q in the green could then be helpful to broaden the bandwidth and satisfy the resonance condition.

The above results support the proposition that the GLC is obtained by THG and third-order SFG. Indeed, as mentioned earlier, these phase-matched frequency-tripling processes take advantage of direct interaction with the strong pump. Therefore, they contribute to the highly-efficient and broadband GLC generation. Based on the experimental results, it seems very likely that the complete GLC could be realized with further optimization of the phase-match condition and the dispersion characteristic, as well as by using stronger pump power. For example, reducing the order of designed phase-matched modes and the difference of effective indices between the fundamental and higher-order modes can attain larger modal overlap in spatial and frequency domain, and consequently increase the conversion bandwidth and efficiency. Moreover, in case of a soliton pulse traveling in the cavity, the higher intensity peak will lead to reduced noise and an even stronger conversion efficiency.

5. Conclusions and outlook

We report frequency comb conversion in an integrated high-Q Si_3N_4 ring microresonator, from IR to the green spectral region through parametric non-linear processes of THG and third-order SFG. Using techniques such as parametric seeding, δ-Δ matching or soliton formation, these mechanisms can be used for the generation of coherent combs in the green spectral region. The multiple phase-matching windows designed between the fundamental mode in the IR and higher-order modes in the green spectral region contribute to the broadband and highly-efficient GLC generation. The 1-THz frequency spacing IR comb covers up to 2/3 of an octave, from 144 to 226 THz (or 1327-2082 nm), and the simultaneously generated GLC is centered around 570-580 THz (or 517-526 nm), with comb lines emitted down to 517 THz (or 580 nm) and up to 597 THz (or 502 nm). The power of the GLC in the bus waveguide is estimated to be as high as -9.1 dBm (or 123 μW), with a conversion efficiency of about -34 dB (or $4 \cdot 10^{-4}$). This approach substantiates the feasibility of Si-based on-chip OFC generation expanding to the green spectral region or even to larger frequencies. We believe this research will expand the insights of a coherent link creation between the visible and IR, motivate the research interest in this area, and trigger the exploration of important applications.

References

[1] D. J. Moss, R. Morandotti, A. L. Gaeta, and M. Lipson, Nature Photon. **7,** 597–607 (2013).

[2] M. J. R. Heck, J. F. Bauters, M. L. Davenport, D. T. Spencer, and J. E. Bowers, Laser Photon. Rev. **8,** 667–686 (2014).

[3] W. Bogaerts, P. De Heyn, T. Van Vaerenbergh, K. De Vos, S. Kumar Selvaraja, T. Claes, P. Dumon, P. Bienstman, D. Van Thourhout, and R. Baets, Laser Photon. Rev. **6,** 47–73 (2012).

[4] M. Aspelmeyer, T. J. Kippenberg, and F. Marquardt, Rev. Mod. Phys. **86,** 1391–1452 (2014).

[5] K. J. Vahala, Nature **424,** 839–846 (2003).

[6] D. T. Spencer, J. F. Bauters, M. J. R. Heck, and J. E. Bowers, Optica **1,** 153–157 (2014).

[7] T. J. Kippenberg, R. Holzwarth, and S. A. Diddams, Science **332,** 555–559 (2011).

[8] A. G. Griffith, R. K. W. Lau, J. Cardenas, Y. Okawachi, A. Mohanty, R. Fain, Y. H. D. Lee, M. Yu, C. T. Phare, C. B. Poitras, A. L. Gaeta, and M. Lipson, Nat. Commun. **6,** 6299 (2015).

[9] C. Reimer, M. Kues, L. Caspani, B. Wetzel, P. Roztocki, M. Clerici, Y. Jestin, M. Ferrera, M. Peccianti, A. Pasquazi, B. E. Little, S. T. Chu, D. J. Moss, and R. Morandotti, Nat. Commun. **6,** 8236 (2015).

[10] C. Y. Lee, C. C. Chang, H. C. Liang, and Y. F. Chen, Laser Photon. Rev. **8,** 750–755 (2014).

[11] X. Xue, Y. Xuan, P. H. Wang, Y. Liu, D. E. Leaird, M. Qi, and A. M. Weiner, Laser Photon. Rev. **9,** 23–28 (2015).

[12] S. A. Diddams, D. J. Jones, J. Ye, S. T. Cundiff, J. L. Hall, J. K. Ranka, R. S. Windeler, R. Holzwarth, T. Udem, and T. W. Hänsch, Phys. Rev. Lett. **84,** 5102–5105 (2000).

[13] S. B. Papp, K. Beha, P. Del'Haye, F. Quinlan, H. Lee, K. J. Vahala, and S. A. Diddams, Optica **1,** 10–14 (2014).

[14] Y. Okawachi, K. Saha, J. S. Levy, Y. H. Wen, M. Lipson, and A. L. Gaeta, Opt. Lett. **36,** 3398–3400 (2011).

[15] T. Herr, K. Hartinger, J. Riemensberger, C. Y. Wang, E. Gavartin, R. Holzwarth, M. L. Gorodetsky, and T. J. Kippenberg, Nature Photon. **6,** 480–487 (2012).

[16] T. Herr, V. Brasch, J. D. Jost, C. Y. Wang, N. M. Kondratiev, M. L. Gorodetsky, and T. J. Kippenberg, Nature Photon. **8,** 145–152 (2014).

[17] F. Ferdous, H. Miao, D. E. Leaird, K. Srinivasan, J. Wang, L. Chen, L. T. Varghese, and A. M. Weiner, Nature Photon. **5,** 770–776 (2011).

[18] J. Pfeifle, V. Brasch, M. Lauermann, Y. Yu, D. Wegner, T. Herr, K. Hartinger, P. Schindler, J. Li, D. Hillerkuss,

R. Schmogrow, C. Weimann, R. Holzwarth, W. Freude, J. Leuthold, T. J. Kippenberg, and C. Koos, Nature Photon. **8**, 375–380 (2014).

[19] S. Miller, K. Luke, Y. Okawachi, J. Cardenas, A. L. Gaeta, and M. Lipson, Opt. Express **22**, 26517–26525 (2014).

[20] J. P. Epping, T. Hellwig, M. Hoekman, R. Mateman, A. Leinse, R. G. Heideman, A. van Rees, P. J. van der Slot, C. J. Lee, C. Fallnich, and K. J. Boller, Opt. Express **23**, 19596–19604 (2015).

[21] H. Zhao, B. Kuyken, S. Clemmen, F. Leo, A. Subramanian, A. Dhakal, P. Helin, S. Severi, E. Brainis, G. Roelkens, and R. Baets, Opt. Lett. **40**, 2177–2180 (2015).

[22] H. Jung, R. Stoll, X. Guo, D. Fischer, and H. X. Tang, Optica **1**, 396–399 (2014).

[23] J. S. Levy, M. A. Foster, A. L. Gaeta, and M. Lipson, Opt. Express **19**, 11415–11421 (2011).

[24] J. D. Jost, T. Herr, C. Lecaplain, V. Brasch, M. H. P. Pfeiffer, and T. J. Kippenberg, arXiv:1411.1354 (2014).

[25] M. H. P. Pfeiffer, A. Kordts, V. Brasch, M. Zervas, M. Geiselmann, J. D. Jost, and T. J. Kippenberg, Optica **3**, 20–25 (2016).

[26] A. Kordts, M. H. P. Pfeiffer, H. Guo, V. Brasch, and T. J. Kippenberg, arXiv:1511.05381 (2015).

[27] V. Brasch, M. Geiselmann, T. Herr, G. Lihachev, M. H. P. Pfeiffer, M. L. Gorodetsky, and T. J. Kippenberg, Science (2015).

[28] A. A. Savchenkov, A. B. Matsko, W. Liang, I. V. S., S. D., and M. L., Nature Photon. **5**, 293–296 (2011).

[29] www.photond.com.

[30] T. Carmon, L. Yang, and K. J. Vahala, Opt. Express **12**, 4742–4750 (2004).